Iran Polym J (2017) 26:179–191
DOI 10.1007/s13726-017-0506-4

ORIGINAL RESEARCH

Shape stability enhancement of PVDF electrospun polymer electrolyte membranes blended with poly(2-acrylamido-2-methylpropanesulfonic acid lithium)

Wei-Wei Cui[1] · Dong-Yan Tang[2] · Yi-Shan Lu[1] · Na Zhang[1] · Li-Zhu Liu[1] · Jin-Long Mu[1]

Received: 23 July 2016 / Accepted: 5 January 2017 / Published online: 2 February 2017

Abstract The purpose of this study is to overcome the poor dimensional stability of poly(vinylidene fluoride) (PVDF)-based electrospun membranes for polymer electrolytes, a new type of composite fibrous membranes based on PVDF/poly(2-acrylamido-2-methylpropanesulfonic acid lithium) (PAMPSLi) blend systems with different blend ratios were fabricated by electrospinning method. Morphology of the composite fibrous membranes was evaluated by scanning electron microscopy. Average diameters of the membranes were less than 250 nm, which were far less than that of pure PVDF fibrous membrane (400 nm). Fourier transform infrared spectroscopy and Raman scattering were used to characterize the interactions of two polymers. Wide-angle X-ray diffraction and differential scanning calorimetry techniques were applied to investigate the crystal structure of composite fibrous membranes. Owning to the good miscibility between PVDF and PAMPSLi, no phase-separated microstructure was observed in composite fibrous membranes. The membranes possessed a good wettability by liquid electrolytes and exhibited an excellent dimensional stability even at high loading of electrolytes. The polymer electrolyte showed the ionic conductivity of 3.45×10^{-3} S/cm at room temperature and electrochemical stability up to 5.4 V for the blend ratio of 5/1. PVDF/PAMPSLi (5/1)-based polymer electrolyte was observed much more suitable than polymer electrolytes with other ratios of PVDF/PAMPSLi for application in high-performance lithium rechargeable batteries.

Keywords Polymer electrolyte · Dimensional stability · Electrospun · PVDF · 2-Acrylamido-2-methylpropanesulfonic acid

Introduction

Recently, polymer electrolytes are widely explored as key materials for the development of various electrochemical devices, such as rechargeable lithium or lithium ion batteries, super capacitors, and fuel cells [1–3]. Among many kinds of polymer electrolytes reported, fibrous polymer electrolytes fabricated by electrospinning polymers, such as poly(vinylidene fluoride) (PVDF) [4, 5], poly(vinylidene fluoride-*co*-hexafluoropropylene) (P(VdF-HFP)) [6, 7], and polyacrylonitrile (PAN) [8, 9] have received a great attention because of their high porosity and ionic conductivity at room temperature. On account of its appealing properties, such as high thermal stability, strong chemical resistance, and high dielectric constant ($\varepsilon \approx 8.4$), PVDF has been in the spotlight as polymer matrices for electrospun fibrous polymer electrolytes [10]. PVDF-based electrospun membranes possess high flatness and evenness as well as good mechanical strength. Meanwhile, the membranes can load large amounts of liquid electrolyte because of the large specific surface area and the high affinity to the liquid electrolyte. As a result, the polymer electrolytes based on PVDF electrospun membranes could achieve high ionic conductivity and excellent electrochemical stability.

Although PVDF-based electrospun membranes exhibit many excellent performances, their wide applications are hindered by the restrained mechanical properties to achieve

✉ Wei-Wei Cui
cuiww@hrbust.edu.cn

[1] College of Materials Science and Engineering, Harbin University of Science and Technology, Harbin 150001, China

[2] Department of Chemistry, School of Science, Harbin Institute of Technology, Harbin 150001, China

high ionic conductivity [11]. After soaking in the liquid electrolyte, the membranes swirl without keeping their original shape, which brings difficulty for assembling lithium-ion batteries. The roughly inverse relationship between the shape stability and conductivity makes it difficult to optimize both mechanical property and ionic conductivity. Many methods have been explored to improve the mechanical property of the polymer electrolytes while keeping high ionic conductivity at the same time. Lee et al. [12] reported that thermal treatment under high pressure made the mechanical properties of electrospun PVDF polymer electrolytes better. However, this occurred at the expense of higher crystallinity, which decreased the liquid electrolyte-absorbing capacity of the membranes. Yee et al. [13] improved the mechanical properties by supercritical carbon dioxide ($SCCO_2$) treatment. This method has made no significant impact on the crystalline structure of the electrospun PVDF membranes, but the amounts of the liquid electrolyte held in the treated membranes were smaller than those in the untreated one. Fang et al. [14] prepared a composite separator consisting of PVDF and montmorillonite (MMT), the membrane had good mechanical properties and high ionic conductivity.

It is well known that polymer blending is a flexible and effective approach to obtain novel materials with complementary advantages of each individual polymer [15]. Based on good solvent resistance in liquid electrolyte [16], PAMPSLi was chosen to endow the blend system with a good mechanical strength. Furthermore, amide and sulfonate groups within AMPS unit make the polymer highly polar and help the dissociation of lithium salts and further improve the ionic conductivity of the system [17, 18]. In this work, an attempt was made to develop a new type of composite fibrous membranes based on PVDF/poly(2-acrylamido-2-methylpropanesulfonic acid lithium) (PAMPSLi) blend system through electrospinning method. The composite fibrous membranes are expected to improve the mechanical properties while retaining a high ionic conductivity. The structures and properties of the membranes were examined systematically and the electrochemical properties of their related polymer electrolytes were investigated.

Experimental

Materials

PVDF (KYNAR 761, ARKEMA, France) was purchased from Cmdic Xiamen Imp. & Exp. Co., Ltd. 2-Acrylamido-2-methylpropanesulfonic acid (AMPS) (99%) was supplied by Henan Huixian ZX Chemical Engineering Co., Ltd (China). Lithium carbonate (Li_2CO_3), *N*,*N*-dimethylformamide (DMF) and azobisisobutyronitrile (AIBN) were analytical reagents grade (China) and used without further purification. Liquid electrolyte [1 mol/L $LiPF_6$ in a 1:1 (wt/wt) mixture of ethylene carbonate (EC) and dimethyl carbonate (DMC)] was supplied by Zhangjiagang Guotai-Huarong New Chemical Materials Co., Ltd (China).

Synthesis of PAMPSLi and blending with PVDF

PAMPSLi was firstly prepared by free radical polymerization of the monomer 2-acrylamido-2-methylpropanesulfonic acid lithium (AMPSLi) with AIBN as the initiator. Detailed procedures are described as follows. The monomer AMPSLi was prepared by the reaction of AMPS with Li_2CO_3 in a DMF solution at ambient temperature. AMPS of 0.03 mol was dissolved in 25.6 g of DMF solvent in a 50 mL beaker at ambient temperature. Li_2CO_3 of 0.015 mol was added slowly into the beaker and stirred until no bubble was formed. The solution was transferred into a three mouth bottle. The initiator AIBN (1% of AMPS weight) was added into the bottle and dissolved completely. The polymerization was carried out at 75 °C for 5 h after the solution was purged with nitrogen for 10 min. The solvents were mainly removed by vacuum distillation, and the residue was poured into a large excess of cold acetone to precipitate the polymer. The polymer (PAMPSLi) was dried in an oven at 80 °C until the weight was unchanged. A certain amount of PAMPSLi was dissolved in DMF to obtain a 20 wt% PAMPSLi solution. Adequate amounts of PVDF powder were dissolved in DMF solution under stirring at 60 °C for 3 h to form a 20 wt% solution. The PVDF solution and the PAMPSLi solution with different PVDF/PAMPSLi ratios of 1/0, 10/1, 5/1, 2/1 and 1/1 (wt/wt) were mixed thoroughly at room temperature to form the composite electrospinning solutions with the concentration of 20 wt%.

Preparation of PVDF/PAMPSLi composite fibrous polymer electrolytes

The composite electrospinning solutions were held in a 5-mL syringe and delivered into a stainless steel needle by a syringe pump (RWDLife Science RWD202, China) with a flow rate of 0.003 mL/min. The needle was connected to an electrode with a high voltage supply, and a ground aluminum foil was placed at 20 cm distance from the needle tip to collect the fibrous membranes. The positive voltage applied to the needle was 14 kV. The environmental temperature was kept at 20 ± 2 °C, and the environmental humidity was kept at 15 ± 1%. After electrospinning, the membranes were dried in an oven at 80 °C for 72 h to remove the remaining solvent. The PVDF/PAMPSLi composite fibrous polymer electrolytes were obtained by soaking the electrospun membranes into a liquid electrolyte

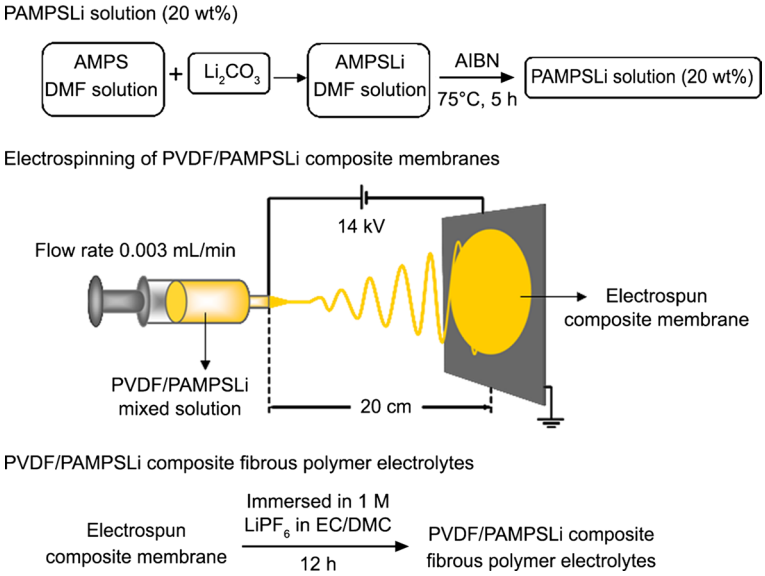

Fig. 1 Schematic representation for the fabrication of PVDF/PAMPSLi composite fibrous polymer electrolytes

of 1 M $LiPF_6$ in 1:1 EC:DMC (wt/wt) for 12 h in a dry glove box. The methodology adopted for the fabrication of PVDF/PAMPSLi composite fibrous polymer electrolytes is presented in Fig. 1.

Characterization and measurements

Scanning electron microscopy (SEM) images were obtained using an FEI Quanta 200 FEG scanning electron microscope (USA) after the samples were sputtered with a thin layer of Pt. Fourier transform infrared (FTIR) spectra of electrospun membranes were obtained on a Nicolet AVATAR 360 system (USA). Dried solids were pressed with KBr and the discs were scanned in the range of 4000–400 cm^{-1} with a resolution of 2 cm^{-1}. The Raman scattering measurements were performed on a JY-HR800 Raman system (France) with a confocal microscopy. The solid-state diode laser (633 nm) was used as an excitation source, and the spectral resolution was set to 1 cm^{-1}. The wide-angle X-ray diffraction (WXRD) was carried on a Rigaku D/MAX-RB X-ray diffractometer (Japan) recorded using Cu Kα radiation at 40 kV and 50 mA. The sample was scanned in the range 5–80° with a step width of 0.02°. The crystallinity of the electrospun membranes were measured on a Netzsch STA 449C differential scanning calorimeter (DSC, Germany) with a heating rate of 10 °C/min under argon atmosphere. The wettability of the membranes was investigated by liquid electrolyte contact angle measurement. The testing was measured using a 2 μL liquid electrolyte droplet on the surface of the membranes under ambient conditions with a Powereach JC2000C Optical Contact Angle Meter (China). The images were captured in continuous shooting mode with interval of 20 ps^{-1}. The uptake of the liquid electrolyte was measured by soaking the electrospun membranes in the liquid electrolyte and weighing at regular intervals after removing the excess liquid electrolyte by wiping with tissue paper. The liquid electrolyte uptake was calculated using the following equation:

$$\varepsilon\ (\%) = \left(\frac{M - M_0}{M_0}\right) \times 100, \tag{1}$$

where ε as the uptake of the liquid electrolyte; M_0, the mass of the membrane, and M as the mass of the membrane after being soaked in liquid electrolyte. The mechanical property and shape stability of electrospun membranes after loading the liquid electrolyte were evaluated by observing their shape change. The membranes were first cut into 45 mm × 20 mm (length and width), and then immersed into the electrolytes for 10 min. The ionic conductivities and electrochemical stability of polymer electrolytes were measured using electrochemical station (CHI 650D, USA). The ionic conductivities were measured by AC impedance method in the frequency range of 0.01–1 MHz. The samples were sandwiched between two stainless steel (SS) plates as blocking electrodes and were kept at each measuring temperature for 30 min to ensure thermal equilibration of the sample at given temperature before measurement. Electrochemical stability was determined using linear sweep voltammetry (LSV) with stainless steel (SS) as a working electrode and lithium as a reference electrode/counter electrode at the scan rate of 1 mV/s over the potential range of 2–6 V at room temperature.

Results and discussion

Characterization of composite fibrous membranes based on PVDF/PAMPSLi

Morphology

Figure 2 presents the SEM images of the PVDF/PAMPSLi-based composite fibrous membranes with different blend ratios and the corresponding fiber diameter distributions. It is clear to note from the images that all of the membranes are made up of fibers without beads, and the fibers are of circular shape in cross-section. The interlaying fibers generate lots of fully interconnected pores, which make them suitable for application as the host matrices for polymer electrolytes. As shown in the Fig. 2a, when the blend ratio of PVDF/PAMPSLi is 1/0, the fibrous membrane has a nearly straightened and tubular structure with an average diameter of about 400 nm. Other composite fibrous membranes shown in Fig. 2b–e have much lower average fiber diameters (less than 250 nm) and more entanglements between these ultrafine fibers, which generates more microcavities in the membranes. The fiber diameters are found to decrease with the changing the blend ratios from 1/0 to 5/1. But it increases again when the blend ratios change to 2/1. The membrane with the blend ratio of 5/1 possesses the smallest fibers (the average diameter of 0.145 μm) and the narrowest fiber diameter distributions (as shown in Fig. 2c′). It is generally known that the factors such as the distance between the nozzle of the syringe and the collector, applied voltage, the concentration of the polymer solution, and the dielectric constant of the solvent are the major parameters that influence the morphology of electrospun fibers. Herein, all the factors in the above list are maintained constant during electrospinning, and hence they cannot be the reason for subsequent morphological differences. So we envisage the following reasons. The incorporation of PAMPSLi increases the charge density of the electrospinning solution due to the partial dissociation of AMPSLi units. This contributes to increase in the electric field forces acted on the electrospinning solution. Electrospun jets are therefore easily formed (in comparison to PVDF solution with a lesser charge density) at the nozzle of the syringe for PVDF/PAMPSLi solution, which causes the formation of fibers with lower diameter. At the same time, this can be attributed to a higher initial velocity and a bigger accelerator on the jets with the increase of PAMPSLi fractions. Thus, the time for drawing and splitting the jet is shorten, which hinders the reduction in fiber diameter. When the fraction of PAMPSLi is not very high, the elongation effect of the electric field forces on the decrease of the fiber diameter is dominant. The fiber diameters of the composite fibrous membranes decrease with the increase of the PAMPSLi fractions. While the PAMPSLi fractions increase up to a certain value, the elongation effect of the electric field forces on shortening of the drawing time is dominant. The fibers do not have enough time to become thinner before they are solidified on the collector. Consequently, the obtained fibers have a bigger fiber diameter. Thus, adopting the method of increasing PAMPSLi fractions in the blend polymers for decreasing the fiber diameters has both positive and negative effects.

Furthermore, the fibers do not have the phase-separated microstructure even for a high content of PAMPSLi. The good miscibility of PVDF and PAMPSLi may be due to their special chemical structures. PAMPSLi contains amide groups (–CO–NH–) and sulfonate groups ($–SO_3$). PVDF contains the strong electron-withdrawing functional group (–C–F) in the backbone. Hydrogen bonds and other molecular level interactions may be formed in the composite fibers, which are helpful to enhance the miscibility of two polymers. Moreover, the electrospinning conditions, such as high voltage and rapid evaporation of the solvent, also could avoid phase separation and induce phase mixing between PVDF and PAMPSLi. Consequently, electrospun matrices without any microphase separation were obtained.

FTIR and Raman spectroscopy study

FTIR spectra of composite fibrous membranes and PAMPSLi are shown in Fig. 3. The spectrum of pure PVDF fibrous membrane (Fig. 3a) shows the characteristic bands at 1402, 1279, 882, 842, 510, and 472 cm^{-1}. The band at 472 cm^{-1} is assigned to CF_2 wagging vibration [19], band at 510 cm^{-1} to CF_2 bending vibration [20], band at 842 cm^{-1} to CH_2 rocking [21], band at 882 cm^{-1} to CF_2 symmetric stretching vibration [22], band at 1279 cm^{-1} to CF_2 asymmetric stretching vibration [23], and band at 1402 cm^{-1} is assigned to CH_2 wagging vibration [24]. There are obvious changes in the FTIR spectra after PAMPSLi is blended into the polymer matrix. First, two new absorption bands appear at 1655 and 1549 cm^{-1}, which are assigned to C=O stretching vibration and the N–H deformation vibration of amide group in PAMPSLi, respectively. Second, these two bands become broader after blending than the bands in pure PAMPSLi (Fig. 3f). Furthermore, a shift for symmetric stretching vibration of the SO_3 group of PAMPSLi from 1037 to 1053 cm^{-1} was also observed. Meanwhile, the CH_2 wagging vibration band at 1402 cm^{-1} progressively widens, and the intensity of the characteristic bands at 510 and 471 cm^{-1} for PVDF decreases significantly with the increase in PAMPSLi content. These changes can be interpreted in terms of the existence of the possible specific molecular level interactions between the two polymers, such as the hydrogen bond between the strong electron-withdrawing functional group (C–F)

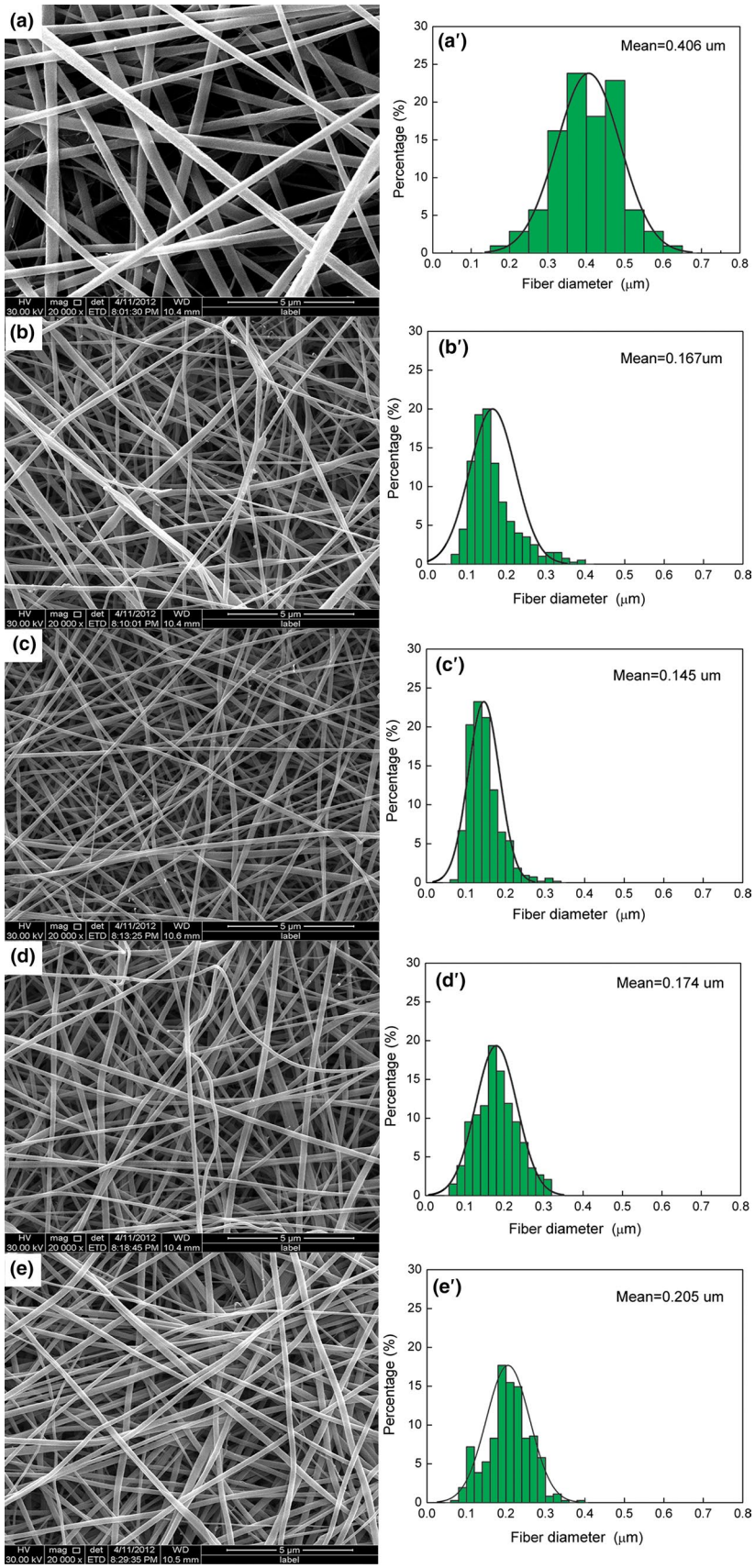

Fig. 2 FESEM images (**a**–**e**) and the corresponding fiber diameter distributions (**a′**–**e′**) of composite fibrous membranes based on PVDF/PAMPSLi with different blend ratios of PVDF/PAMPSLi = 1/0 (**a**, **a′**), 10/1 (**b**, **b′**), 5/1 (**c**, **c′**), 2/1 (**d**, **d′**), and 1/1 (**e**, **e′**)

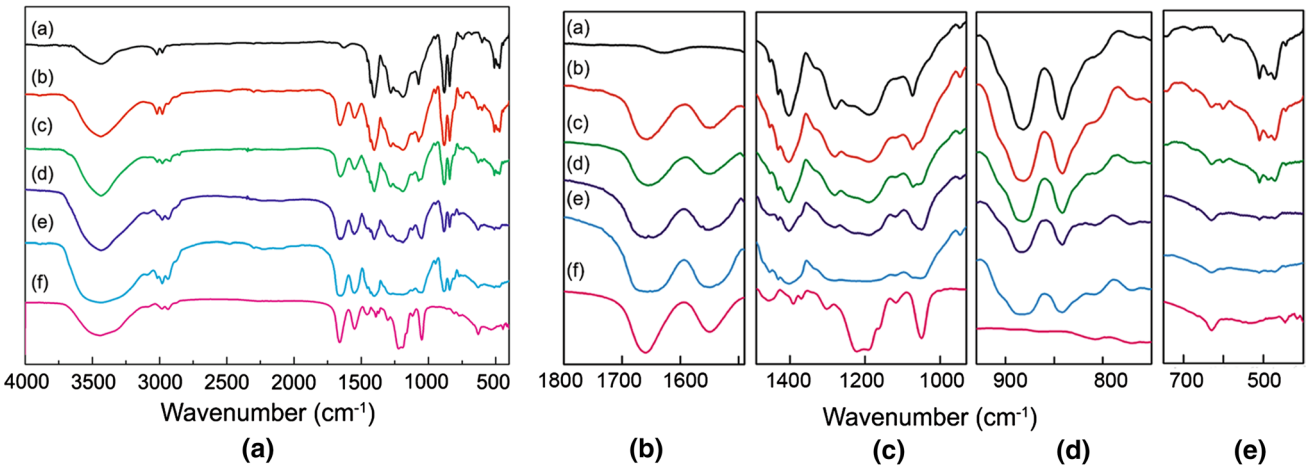

Fig. 3 FTIR spectra at different wavenumber regions: **a** 4000–400 cm^{-1}; **b** (*B*) 1800–1490 cm^{-1}; **b** (*C*) 1490–930 cm^{-1}; **b** (*D*) 930–750 cm^{-1}; and **b** (*E*) 750–400 cm^{-1} for composite fibrous membranes based on PVDF/PAMPSLi with blend ratios PVDF/PAMPSLi = 1/0 (*a*), 10/1 (*b*), 5/1 (*c*), 2/1 (*d*), 1/1 (*e*), and PAMPSLi (*f*)

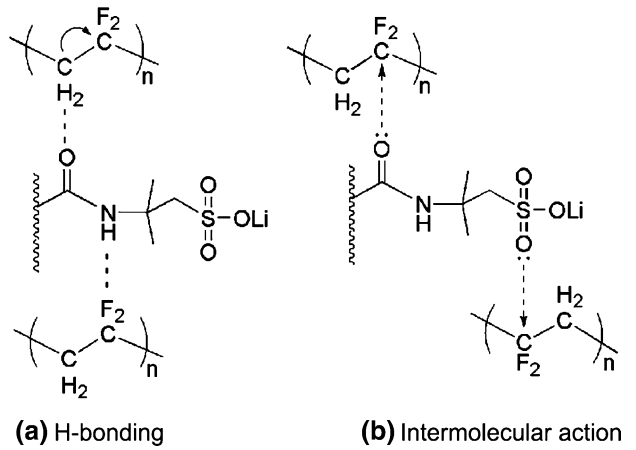

Fig. 4 Schematic model of hydrogen bonds and other possible molecular level interactions between PVDF and PAMPSLi

of PVDF and the imino group (–NH) in the side chain of PAMPSLi, the hydrogen bond between the oxygen in the C=O group of PAMPSLi and the hydrogen in the methylene group of PVDF, the interaction of the C=O group of PAMPSLi and CF_2 group of PVDF, and the interaction of the SO_3 group of PAMPSLi and CF_2 group of PVDF. Similar molecular level interactions were also reported for the blend system of PVDF/poly(vinyl pyrrolidone) (PVP) [25]. These molecular level interactions can only be taken as a probable suggestion for phase mixing between PVDF and PAMPSLi. Schematic model of the interactions is shown in Fig. 4.

Raman data can provide more spectroscopic information than that of IR analysis alone [26]. So to further investigate the structure of fibrous membranes and the interactions between PVDF and PAMPSLi, Raman scattering measurements of pure PVDF fibrous membrane and the composite fibrous membrane with the blend ratio of 2/1 were performed. It is well known that the PVDF chains mainly crystallize into five crystalline forms (α, β, γ, δ and ε) depending on different processing conditions [27]. From the results, shown in Fig. 5, the dominated characteristic bands in the Raman spectrum of pure PVDF fibrous membrane (Fig. 5a) are identified to the characteristic bands of β-phase of PVDF. The band at 260 cm^{-1} is assigned to CF_2 twisting vibration, 512 cm^{-1} to the CF_2 scissoring vibration, 840 cm^{-1} to a mixed mode of CH_2 rocking and CF_2 asymmetric stretching vibration, 881 cm^{-1} to a mixed mode of CC asymmetric stretching vibration and CF_2 symmetric stretching vibration, and 1279 cm^{-1} to a mixed mode of CF_2 asymmetric stretching vibration and CC symmetric stretching vibration [28]. Among these bands, the band at 840 cm^{-1} provides the most remarkable information with the high intensity confirming the high percentage of β-phase in membrane [29]. So the spectrum reveals that the membrane mainly contains the β-phase crystal structure of PVDF. Other bands at 1073, 1431, 2977, and 3014 cm^{-1} are assigned to the mixed mode of CC asymmetric stretching and CF_2 wagging and CH_2 wagging vibration, the mixed mode of CH_2 scissoring and CH_2 wagging vibration, CH_2 symmetric stretching vibration and CH_2 asymmetric stretching vibration, respectively. For the PVDF/PAMPSLi (2/1) composite fibrous membrane, several new bands appeared at 778, 1047, and 2940 cm^{-1} are identified for the NH stretching vibration in PAMPSLi, the $–SO_3$ symmetric stretching vibration, and the CH_2 symmetric stretching vibration, respectively [30]. Although the β-phase crystal structure of PVDF still predominates, the intensity of the corresponding bands decreases (especially for that at 840 cm^{-1}), which indicates that the crystallinity

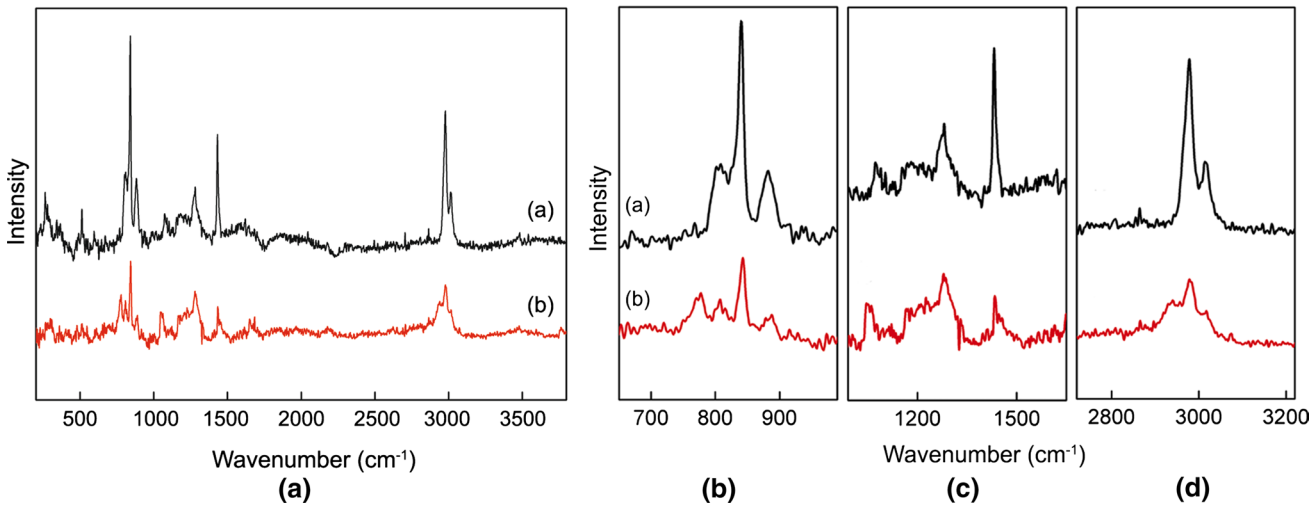

Fig. 5 Raman spectra at different wavenumber regions **a** 200–3800 cm^{-1}; **b** (*B*) 650–990 cm^{-1}; **b** (*C*) 990–1650 cm^{-1}; and **b** (*D*) 2720–3220 cm^{-1} for composite fibrous membranes based on PVDF/PAMPSLi with blend ratios PVDF/PAMPSLi = 1/0 (*a*) and 2/1 (*b*)

of PVDF declines. Furthermore, the band at 840 cm^{-1} for pure PVDF electrospun membrane shifts to 843 cm^{-1} for the composite fibrous membrane, and the band at 881 cm^{-1} shifts to 888 cm^{-1}. The further shift confirms the existence of hydrogen bonds and other molecular level interactions between PVDF and PAMPSLi.

Crystalline structure and thermal properties

The results of XRD patterns are shown in Fig. 6. The strong diffraction peak observed at 2θ of 20.7° for all the electrospun membranes corresponds to 110 and 200 reflections of β-phase and indicates the dominance of β-phase in the electrospun membranes [31]. The intensity of the diffraction peak declines sharply with the increase of PAMPSLi content. During electrospinning, polymer solution experiences two forces: one is shear force when it flows through a needle. The other one is columbic force when the jet is elongated and accelerated by the high electric field applied. The combination of the two forces induces disentanglement and parallel packing of polymer chains, and facilitates the orientation of the chains along the fibrous axis. Hence, large numbers of β-phases are formed. Enhancing the PAMPSLi fraction in the blending polymers results in the increase of hydrogen bonds and molecular level interactions between PVDF and PAMPSLi, which hinder the motion of polymer segments and the orientation of the chains along the fibrous axis. So the intensity of the diffraction peak with the membrane composition decreases.

DSC measurements were used to investigate the variation of crystallinity of the composite fibrous membranes with the blending ratio, and the results are shown in Fig. 7. It is observed that all curves have almost similar

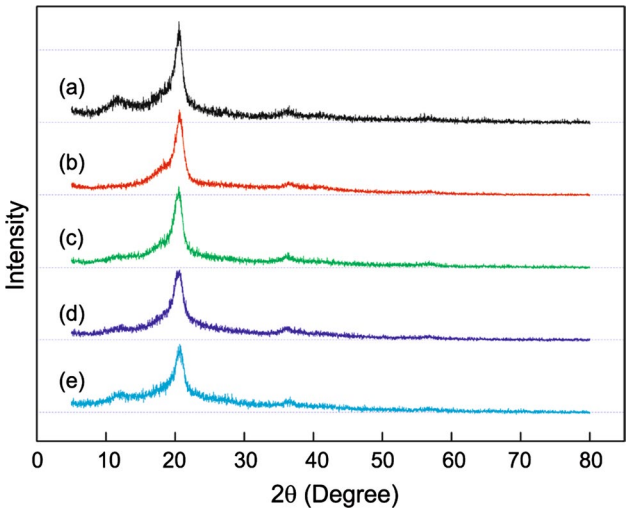

Fig. 6 WAXD patterns of composite fibrous membranes based on PVDF/PAMPSLi with different blend ratios, PVDF/PAMPSLi = 1/0 (*a*), 10/1 (*b*), 5/1 (*c*), 2/1 (*d*), and 1/1 (*e*)

endothermic peaks. The endothermic peaks extend from 150 to 185 °C with a peak at 170 °C, corresponding to the β-phase fusion in PVDF [32]. The melting enthalpy (ΔH_f) of the composite fibrous membranes can be calculated from the integral area of the baseline and each melting curve. The reduction of melting enthalpy is evident with the increase of the PAMPSLi fraction. The value of melting enthalpy obtained from their respective DSC curves can determine the crystallinity (X_c) of PVDF by the following formula:

$$\chi_c\ (\%) = \triangle H_f / (\triangle H_f^* \phi) \times 100, \quad (2)$$

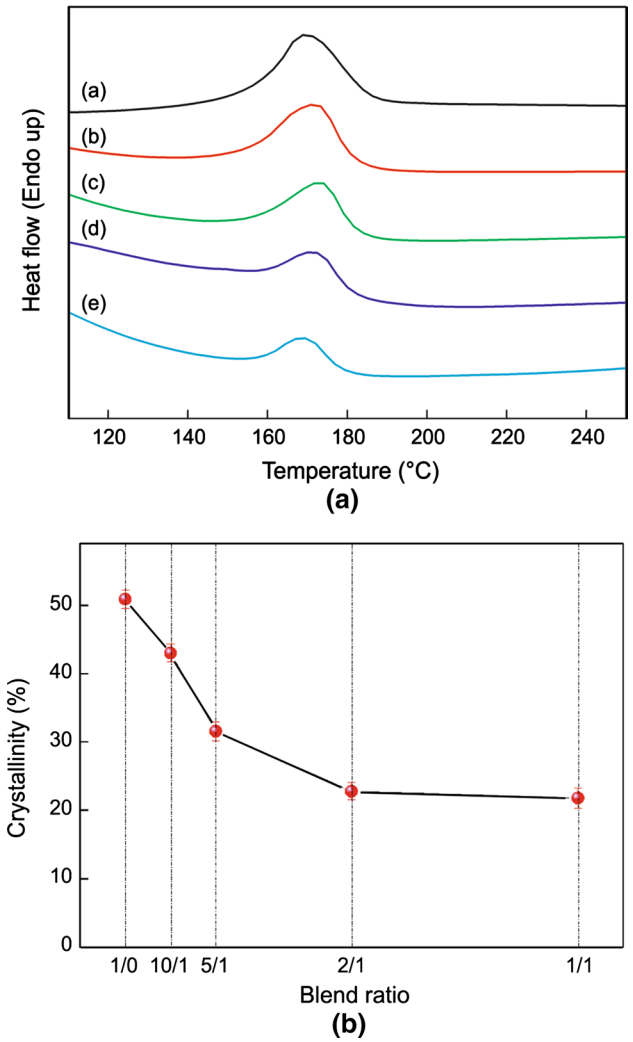

Fig. 7 **a** DSC thermograms of composite fibrous membranes based on PVDF/PAMPSLi with different blend ratios, PVDF/PAMPSLi = 1/0 (*a*), 10/1 (*b*), 5/1 (*c*), 2/1 (*d*), and 1/1 (*e*); and **b** crystallinity data of composite fibrous membranes

where ΔH_f^* is the crystalline melting enthalpy of perfectly crystalline PVDF (104.7 J g^{-1}) [33]. ΔH_f is the melting enthalpy of the electrospun membranes. Φ is the weight fraction of PVDF. The crystallinity values, calculated using Eq. (2), are illustrated in Fig. 7b. Consistent with the results from XRD measurements, it is clear that the crystalline degree of PVDF is reduced by the introduction of PAMPSLi. Compared with 50.9% for pure PVDF fibrous membrane, the crystallinity is reduced to as low as 21.8% for the membranes with 1:1 PVDF:PAMPSLi blend. Such drop in crystallinity should be beneficial to the uptake of liquid electrolyte due to the soaking effect in the amorphous PVDF domain. Moreover, membrane with low crystallinity can supply a beneficial condition for conductivity enhancement. Thus, the results suggest the excellent ionic conductivity of the PVDF/PAMPSLi composite fibrous polymer electrolytes.

Wettability and electrolyte uptake

Membranes with good wettability can retain the electrolyte in the cavity of their porous structure effectively and facilitate an electrolyte to diffuse smoothly into the cell assembly, so the wettability of the membranes by the electrolyte is an important parameter [34]. In this work, the wettability of the electrospun membranes was quantitatively evaluated by measuring the development in contact angles of the liquid electrolyte with time. For comparison, the contact angles of the PE separator (commercial polyolefin-based separator, Celguard 2400) were also investigated. The images of contact angles are shown in Fig. 8a, and the variations of the electrolyte contact angles versus time are summarized in Fig. 8b. The moment that the liquid electrolyte is dripped on the membrane is defined as the initial time. As shown in Fig. 8a(a), after being dripped on the PE separator, the drop keeps the shape of a circular arc. The contact angle maintains at the level of 44° during a 4 s observation, and the magnitude of the drop base diameter does not change with time. This poor wettability results from the large difference of the polarity between the nonpolar polyolefin separator and the highly polar liquid electrolyte, which will result in an increase in cell resistance. In comparison to the PE separator, all the composite fibrous membranes with different PAMPSLi fractions are quickly wetted by the liquid electrolyte. As shown in Fig. 8a(b–g), after being dripped on the electrospun membranes, the drops spread quickly on the surface of membranes, and penetrate into the interior of the membranes within 4 s. The contact angles decrease continuously from about 20° to 0°, and the magnitudes of the drop base diameters increase rapidly with time. The excellent electrolyte wettability of electrospun membranes is attributed to the fully interconnected unique pore structure produced by electrospinning and the affinity between the polymer matrix and the liquid electrolyte, both of which may facilitate capillary intrusion of the liquid electrolyte into the pores [35].

Fibrous polymer electrolytes were prepared by activating the electrospun membranes with the liquid electrolyte of 1 M $LiPF_6$ in EC/DMC (wt/wt). Figure 9 presents the electrolyte uptake behavior of the composite fibrous membranes with different blend ratios. The unique three-dimensional network structure of electrospun membranes enables the easy penetration of liquid into the inner cavities through the interconnected pores, and hence the uptake process becomes stabilized within a short time. All the membranes reported here exhibit the electrolyte uptakes higher than 300%. The uptake is increased up to the blend ratio of 5/1; beyond this threshold a decrease is observed. In detail, when the blend ratios of PVDF/PAMPSLi are in the range of 1/0–5/1, the electrolyte uptake is observed to increase

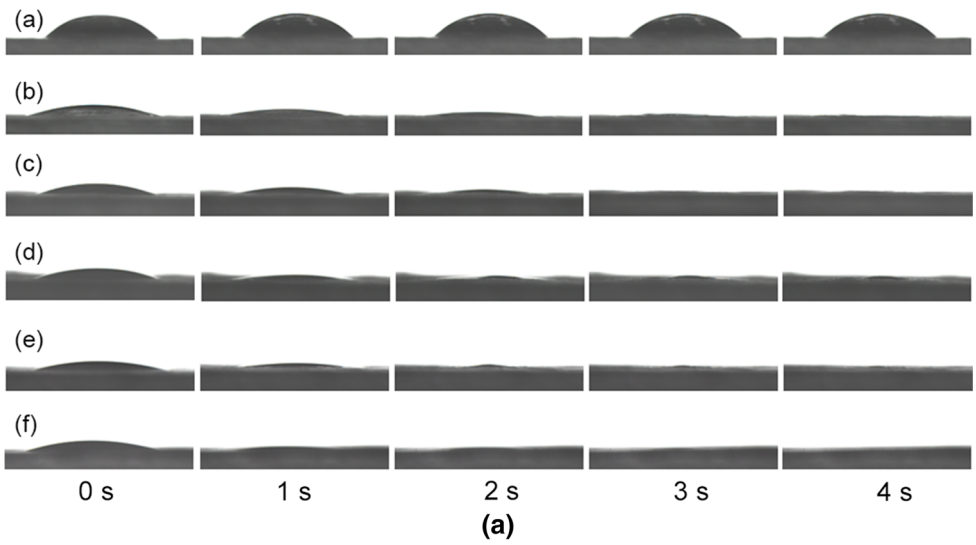

(a)

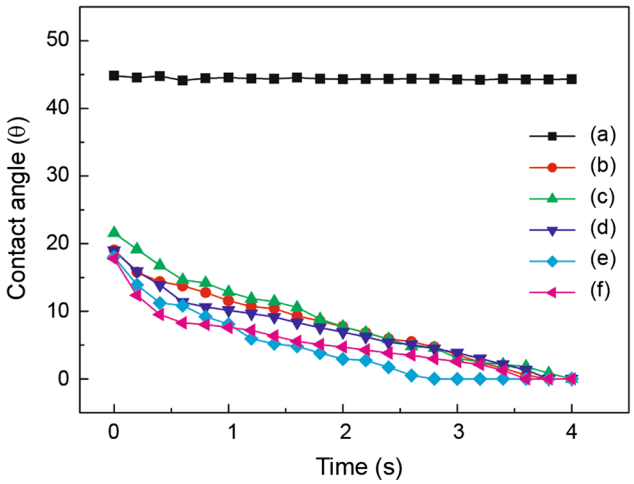

(b)

Fig. 8 Optical photos: **a** the evolution of contact angles; and **b** of the liquid electrolyte with time on PE separator (*a*) and on the composite fibrous membranes based on PVDF/PAMPSLi with different blend ratios, PVDF/PAMPSLi = 1/0 (*b*), 10/1 (*c*), 5/1 (*d*), 2/1 (*e*), and 1/1 (*f*)

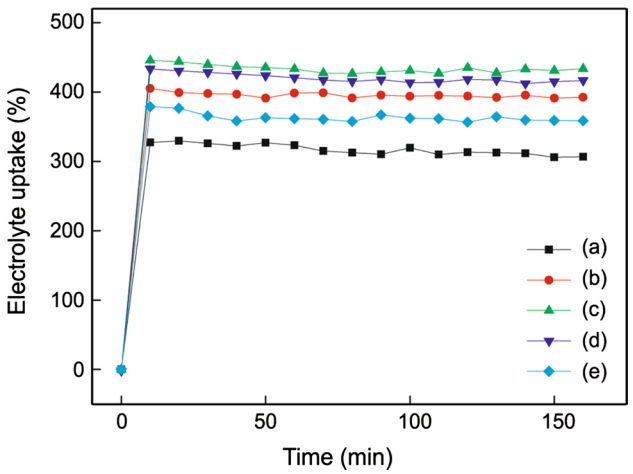

Fig. 9 Electrolyte uptake of composite fibrous membranes based on PVDF/PAMPSLi with different blend ratios [liquid electrolyte: 1 M $LiPF_6$ in EC/DMC (wt/wt)], PVDF/PAMPSLi = 1/0 (*a*), 10/1 (*b*), 5/1 (*c*), 2/1 (*d*), and 1/1 (*e*)

steadily with the PAMPSLi fractions. The uptake obtains the maximum value (up to 430%) with the blend ratio of 5/1. The absorption of large quantities of liquid electrolyte results from a high specific surface area of the membranes and its high amorphous content. The uptake begins to decrease with further increases in blend ratios. While the blend ratio is 1/1, the uptake declines to 360%. This decrease indicates that the favorable properties imparted by PAMPSLi towards electrolyte uptake are masked at a higher content. Previous works on the PVDF–solvent interaction [36] reported that the hydrogen of methylene group in PVDF and the oxygen in the carbonyl group of the carbonate acted as a Lewis acid and a Lewis base, respectively. This specific interaction is weakened by the hydrogen bonds and other molecular level interactions between PVDF and PAMPSLi when the PAMPSLi fractions are further enhanced. So the electrolyte uptake decreases.

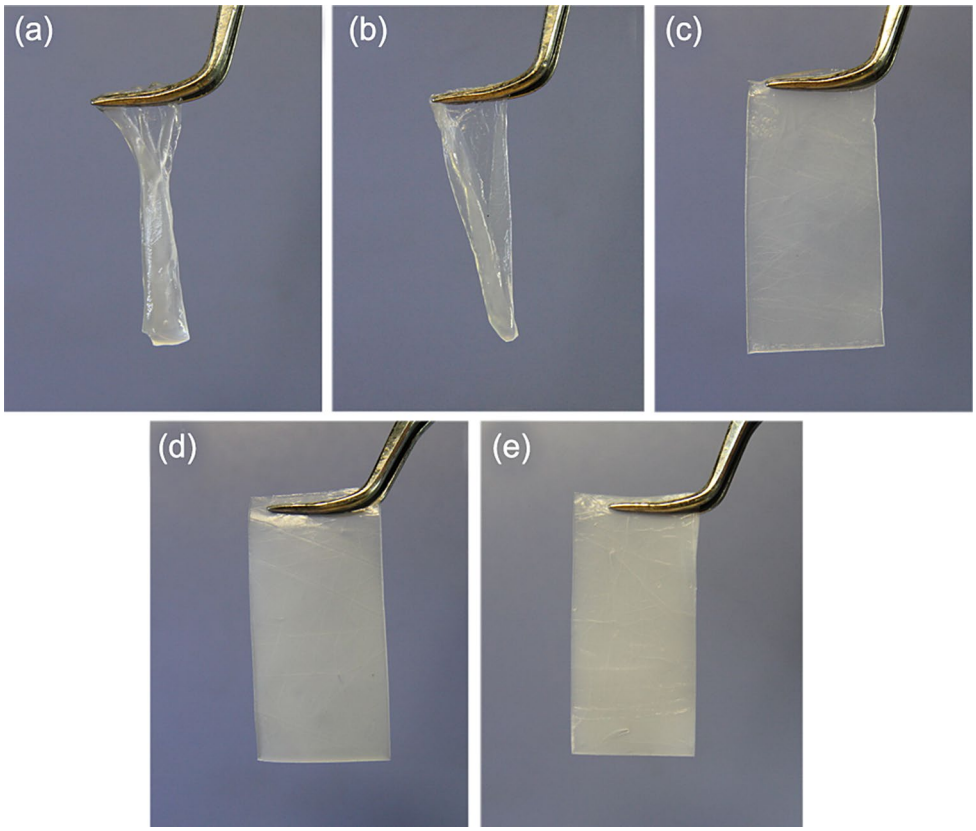

Fig. 10 Dimensional stability of fibrous polymer electrolytes based on PVDF/PAMPSLi with different blend ratios, PVDF/PAMPSLi = 1/0 (**a**), 10/1 (**b**), 5/1 (**c**), 2/1 (**d**), and 1/1 (**e**)

Characteristics of composite fibrous polymer electrolytes

Dimensional stability

The dimensional stability is an essential property for polymer electrolytes in terms of the processibility for practical device fabrication. To investigate the effect of different blend ratios on the dimensional stability of fibrous polymer electrolytes based on PVDF/PAMPSLi, the changes in the shape of the composite fibrous membranes after being activated with the liquid electrolyte are shown in Fig. 10. It can be seen that the pure PVDF fibrous membranes stick together and form a gelled mess, which results in a difficult assembling process of the cells. When the blend ratio of PVDF/PAMPSLi is 10/1, the membrane cannot retain its initial shape, and the problem of poor dimensional stability still exists. While the blend ratios are in the range of 5/1–1/1, the membranes well retain their shape and exhibit sufficient mechanical strength and self-standing properties. When the pure PVDF electrospun membrane is immersed into the liquid electrolyte, a large amount of liquid electrolyte is absorbed into the membrane through capillary action. This results in the strained mechanical properties of the membrane. Consequently, the membrane loses its shape stability. Fortunately, with the PVDF as a main polymer matrix, blending along with PAMPSLi can contribute to the mechanical property for polymer electrolytes. It is considered that the increase of the PAMPSLi fractions can prevent the shape deformation because of its relative poor affinity with electrolyte. Moreover, the hydrogen bonds and other possible molecular level interactions between PVDF and PAMPSLi reduce the interactions between PVDF and the liquid electrolyte, which may be another reason for the improvement of the shape stability.

Ionic conductivity

Figure 11 shows the temperature dependence of ionic conductivity for the PVDF/PAMPSLi-based fibrous polymer electrolytes with different blend ratios of PVDF/PAMPSLi. It is found that the ionic conductivities for all polymer electrolytes are higher than 10^{-3} S/cm in the range of 20–70 °C. The presence of PAMPSLi has a pronounced influence on the conductivities of the polymer electrolytes over the entire temperature range. Figure 11 shows how the ionic conductivity reaches a maximum with blend ratio of PVDF/PAMPSLi, after which it reduces dramatically. In detail, the ionic conductivities at 20 °C are 2.44×10^{-3}, 2.69×10^{-3}, 3.45×10^{-3}, 3.49×10^{-3}, and 2.70×10^{-3} S/cm, respectively, for the fibrous polymer electrolytes with blend ratios of

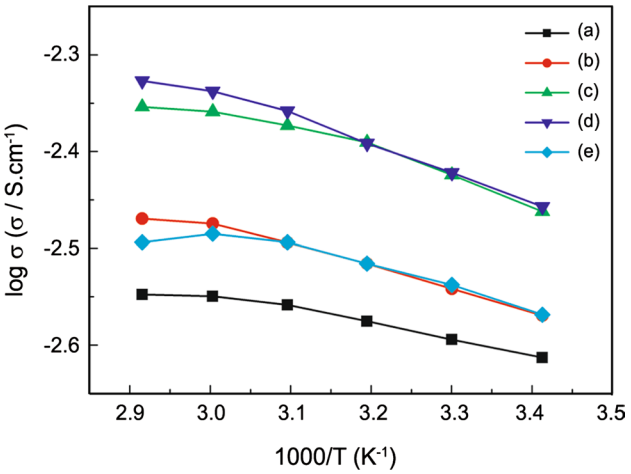

Fig. 11 Temperature dependence of ionic conductivity of fibrous polymer electrolytes based on PVDF/PAMPSLi with different blend ratios, PVDF/PAMPSLi = 1/0 (*a*), 10/1 (*b*), 5/1 (*c*), 2/1 (*d*), and 1/1 (*e*)

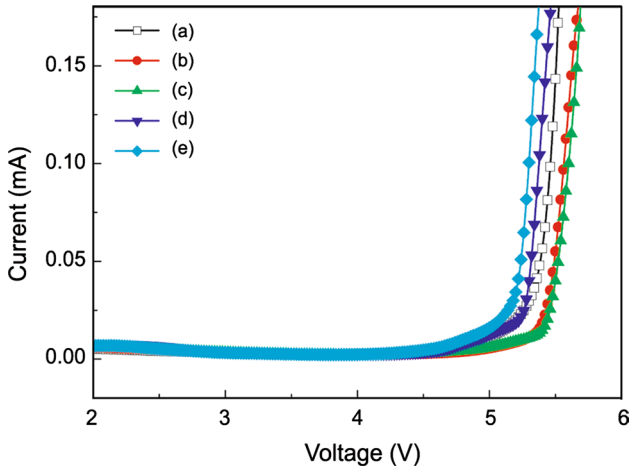

Fig. 12 Anodic stability by LSV of fibrous polymer electrolytes based on PVDF/PAMPSLi with different blend ratios, PVDF/PAMPSLi = 1/0 (*a*), 10/1 (*b*), 5/1 (*c*), 2/1 (*d*), and 1/1 (*e*) (Li/polymer electrolyte/SS cells, 1 mVs^{-1}, 2–6 V)

1/0, 10/1, 5/1, 2/1, and 1/1. The maximum ionic conductivity reaches around the blend ratios of 5/1 and 2/1; they are thought to be the ideal blend ratios in terms of ionic conductivity for this system. Then a decrease in ionic conductivity is seen in the sample with the blend ratio of 1/1. The variation in ionic conductivity may be due to the differences in the structures and the molecular level interactions of polymer electrolytes. There are generally three phases in fibrous polymer electrolytes, like a solid polymer fiber phase, a partially swollen amorphous fiber phase, and a liquid electrolyte phase encapsulated in the pores of the membrane [37]. Among three phases, the liquid electrolyte phase and the swollen polymer phase are the fast and slow conduction paths for ionic conduction, respectively. Herein, the presence of PAMPSLi decreases the fiber diameter, and increases the surface area and the amorphous PVDF domain of the membranes with low PAMPSLi fraction. This helps the fibrous membranes entrap more liquid electrolyte as shown in Fig. 9, and thus the polymer electrolyte with the blend ratio of 5/1 exhibits high ionic conductivity. Although the composite polymer electrolyte with the blend ratio of 2/1 possesses a lower electrolyte uptake than the polymer electrolyte with the blend ratio of 5/1, it still exhibits a high ionic conductivity because of the high polarity of PAMPSLi which is beneficial to the dissociation of lithium salt. In case of the sample with the blend ratio of 1/1, the hydrogen bonds and other possible molecular level interactions between PVDF and PAMPSLi reduce the interactions between PVDF and electrolyte. Therefore, the uptake of the membrane deceases dramatically, which directly leads to reduced ionic conductivity.

Electrochemical stability

Electrochemical stabilities of PVDF/PAMPSLi polymer electrolytes were investigated by LSV method. Figure 12 shows the LSV curves of the polymer electrolytes with different blend ratios. It is known that the increase of current flow in the high voltage results from the decomposition process associated with electrolyte. In addition, the corresponding onset voltage is an upper limit of the electrolyte stability range. As can be seen from Fig. 12, the current through all polymer electrolytes is very small when the cell voltage is lower than 5 V, which indicates that no significant decomposition in components takes place below 5.0 V of the polymer electrolytes. This demonstrates that the polymer electrolytes are very suitable for application in lithium-ion batteries. The polymer electrolyte based on pure PVDF fibrous membrane (PVDF/PAMPSLi = 1/0) exhibits an anodic stability at 5.1 V. With the incorporation of PAMPSLi into the polymer matrix, the electrochemical stability is found to increase up to 5.4 V with the blend ratios of 10/1 and 5/1. Then it decreases to 5.1 V again when the blend ratios increase to 2/1 and 1/1. From Fig. 12, we can see clearly that the polymer electrolyte with the blend ratio of 5/1 shows the best electrochemical stability.

For fibrous polymer electrolytes, the ionic conduction occurs mainly through the entrapped liquid electrolyte in the pore structure. The electrochemical stability is influenced by the fully interconnected pores, specific surface area and the average fiber diameters. Combining the results shown in Fig. 2, it can be concluded that the anodic stability of the polymer electrolytes increases with decreasing average fiber diameters. On the other hand, the carbonate-based liquid electrolyte can partially swell the fibers. The

complex compounds formed in the swollen phase, such as associated VdF-Li^+ groups and the associated VdF–Li^+–OC groups can enhance the electrochemical stability of polymer electrolytes as well as the dipole–dipole interaction between the CO group of the carbonate molecules and the PVDF [36]. Thus, the swollen phase contributes significantly in enhancing the stability of the polymer electrolyte. Combining the results of the DSC measurements, the increase of the PAMPSLi fractions enhances the swollen phase of the fibrous polymer electrolytes, and thereby results in high electrochemical stability. In the case of the further enhancement of the PAMPSLi fractions, the interactions between PVDF and the liquid electrolyte are weakened by the interactions between PVDF and PAMPSLi. Therefore, the decrease in the electrochemical stability is observed.

Conclusion

A series of composite fibrous membranes based on PVDF/PAMPSLi blending system were fabricated by electrospinning 20 wt% polymer solution with different blend ratios. The composite fibrous membranes exhibited smaller fiber diameter and lower crystallinity than the pure PVDF membrane. Meanwhile, they possessed excellent wettability and electrolyte uptake. When the blend ratio was 5/1, the composite fibrous polymer electrolyte not only exhibited much better dimensional stability, but also possessed high ionic conductivity and electrochemical stability. Incorporation of PAMPSLi has been verified to be an effective method in improving the properties of PVDF-based fibrous polymer electrolytes.

Acknowledgements This work was supported by 2014 Heilongjiang Province Education Department Science and Technology Research Project (12541113).

References

1. Okafor PA, Iron JO (2015) Fabrication of porous graphene/polyimide composites using leachable poly-acrylic resin for enhanced electrochemical and energy storage capabilities. J Mater Chem A 3:17230–17240
2. Li W, Wu YH, Wang JW, Huang D, Chen LZ, Yang G (2015) Hybrid gel polymer electrolyte fabricated by electrospinning technology for polymer lithium-ion battery. Eur Polym J 67:365–372
3. Kozakiewicz J, Przybylski J, Sylwestrzak K (2016) Silicone-urethane membranes for lithium batteries. Part 1. moisture-cured poly(siloxane-urethane-urea) elastomers containing polyethylene oxide (PEO) segments—synthesis and characterization as potential membrane materials. Polym Adv Technol 27:258–265
4. Yang CL, Li ZH, Li WJ, Liu HY, Xiao QZ, Lei GT, Ding YH (2015) Batwing-like polymer membrane consisting of PMMA-grafted electrospun PVdF–SiO_2 nanocomposite fibers for lithium-ion batteries. J Membr Sci 495:341–350
5. Wu N, Jing B, Cao Q, Wang XY, Kuang H, Wang Q (2012) A novel electrospun TPU/PVdF porous fibrous polymer electrolyte for lithium ion batteries. J Appl Polym Sci 125:2556–2563
6. Elayappan V, Murugadoss V, Angaiah S, Fei ZF, Dyson PJ (2015) Development of a conjugated polyaniline incorporated electrospun poly(vinylidene fluoride-*co*-hexafluoropropylene) composite membrane electrolyte for high performance dye-sensitized solar cells. J Appl Polym Sci 132:42777(1–8)
7. Padmaraj O, Venkateswarlu M, Satyanarayana N (2014) Characterization and electrochemical properties of P(VdF-*co*-HFP) based electrospun nanocomposite fibrous polymer electrolyte membrane for lithium battery applications. Electroanalysis 26:2373–2379
8. Lee JH, Manuel J, Choi H, Park WH, Ahn JH (2015) Partially oxidized polyacrylonitrile nanofibrous membrane as a thermally stable separator for lithium ion batteries. Polymer 68:335–343
9. Jeong KU, Chae HD, Il Lim C, Lee HK, Ahn JH, Nah C (2010) Fabrication and characterization of electrolyte membranes based on organoclay/tripropyleneglycol diacrylate/poly(vinylidene fluoride) electrospun nanofiber composites. Polym Int 59:249–255
10. Kang GD, Cao YM (2014) Application and modification of poly(vinylidene fluoride) (PVDF) membranes—a review. J Membr Sci 463:145–165
11. Li GC, Li ZH, Zhang P, Zhang HP, Wu YP (2008) Research on a gel polymer electrolyte for Li-ion batteries. Pure Appl Chem 80:2553–2563
12. Lee SW, Choi SW, Jo SM, Chin BD, Kim DY, Lee KY (2006) Electrochemical properties and cycle performance of electrospun poly(vinylidene fluoride)-based fibrous membrane electrolytes for Li-ion polymer battery. J Power Sources 163:41–46
13. Yee WA, Xiong SX, Ding GQ, Nguyen CA, Lee PS, Ma J, Kotaki M, Liu Y, Lu XH (2010) Supercritical carbon dioxide-treated electrospun poly(vinylidene fluoride) nanofibrous membranes: morphology, structures and properties as an ionic-liquid host. Macromol Rapid Commun 31:1779–1784
14. Fang CJ, Yang SL, Zhao XF, Du PF, Xiong J (2016) Electrospun montmorillonite modified poly(vinylidene fluoride) nanocomposite separators for lithium-ion batteries. Mater Res Bull 79:1–7
15. Prateek Thakur VK, Gupta RK (2016) Recent progress on ferroelectric polymer-based nanocomposites for high energy density capacitors: synthesis, dielectric properties, and future aspects. Chem Rev 116:4260–4317
16. Cui WW, Tang DY, Gong ZL, Guo YD (2012) Performance enhancement induced by electrospinning of polymer electrolytes based on poly(methyl methacrylate-*co*-2-acrylamido-2-methylpropanesulfonic acid lithium). J Mater Sci 47:6276–6285
17. Zygadlo-Monikowska E, Florjanczyk Z, Wielgus-Barry E, Pasniewski J (2006) Proton conducting gel polyelectrolytes based on 2-acrylamido-2-methyl-1-propanesulfonic acid (AMPSA) copolymers with polyfunctional monomers. Part I. anhydrous systems. J Power Sources 159:385–391
18. Choi DI, Ryu SW (2015) Effect of BF3 inclusion on poly(POEM-*co*-AMPSLi) single-ion polymer electrolytes. Polym Korea 39:621–626
19. Thankamony RL, Chu H, Lim S, Yim T, Kim YJ, Kim TH (2015) Preparation and characterization of imidazolium-PEO-based ionene/PVDF(HFP)/LiTFSI as a novel gel polymer electrolyte. Macromol Res 23:38–44
20. Upadhyay RH, Deshmukh RR (2013) Investigation of dielectric properties of newly prepared beta-phase polyvinylidene fluoride–barium titanate nanocomposite films. J Electrostat 71:945–950
21. Rana DS, Chaturvedi DK, Quamara JK (2009) Morphology, crystalline structure, and chemical properties of 100 MeV

Ag- ion beam irradiated polyvinylidene fluoride (PVDF) thin film. J Optoelectron Adv Mater 11:705–712
22. Kobayashi M, Tashiro K, Tadokoro H (1975) Molecular vibrations of three crystal forms of poly (vinylidene fluoride). Macromolecules 8:158–171
23. Lanceros-Mendez S, Mano JF, Costa AM, Schmidt VH (2001) FTIR and DSC studies of mechanically deformed beta-PVDF films. J Macromol Sci Phys B 40:517–527
24. Song LZ, Zhang ZJ, Song SZ, Gao ZM (2007) Preparation and characterization of the modified polyvinylidene fluoride (PVDF) hollow fibre microfiltration membrane. J Mater Sci Technol 23:55–60
25. Chen NP, Hong L (2002) Surface phase morphology and composition of the casting films of PVDF-PVP blend. Polymer 43:1429–1436
26. Nallasamy P, Mohan S (2005) Vibrational spectroscopic characterization of form II poly(vinylidene fluoride). Indian J Pure Appl Phys 43:821–827
27. Boudriaux M, Rault F, Cochrane C, Lemort G, Campagne C, Devaux E, Courtois C (2016) Crystalline forms of PVDF fiber filled with clay components along processing steps. J Appl Polym Sci 133:43244(1–9)
28. Bao SP, Liang GD, Tjong SC (2011) Effect of mechanical stretching on electrical conductivity and positive temperature coefficient characteristics of poly(vinylidene fluoride)/carbon nanofiber composites prepared by non-solvent precipitation. Carbon 49:1758–1768
29. Satapathy S, Pawar S, Gupta PK, Varma KBR (2011) Effect of annealing on phase transition in poly(vinylidene fluoride) films prepared using polar solvent. Bull Mater Sci 34:727–733
30. Yang CC, Lue SJ, Shih JY (2011) A novel organic/inorganic polymer membrane based on poly(vinyl alcohol)/poly(2-acrylamido-2-methyl-1-propanesulfonic acid/3-glycidyloxypropyl trimethoxysilane polymer electrolyte membrane for direct methanol fuel cells. J Power Sources 196:4458–4467
31. Yang JH, Feng CX, Chen HM, Zhang N, Huang T, Wang Y (2016) Toughening effect of poly(methyl methacrylate) on an immiscible poly(vinylidene fluoride)/polylactide blend. Polym Int 65:675–682
32. Medeiros AS, Gual MR, Pereira C, Faria LO (2015) Thermal analysis for study of the gamma radiation effects in poly (vinylidene fluoride). Radiat Phys Chem 116:345–348
33. Shimizu H, Arioka Y, Ogawa M, Wada R, Okabe M (2011) Sol–gel transitions of poly(vinylidene fluoride) in organic solvents containing LiBF4. Polym J 43:540–544
34. Chen WJ, Shi LY, Wang ZY, Zhu JF, Yang HJ, Mao XF, Chi MM, Sun LN, Yuan S (2016) Porous cellulose diacetate-SiO_2 composite coating on polyethylene separator for high-performance lithium-ion battery. Carbohydr Polym 147:517–524
35. Lee T, Kim WK, Lee Y, Ryou MH, Lee YM (2014) Effect of Al_2O_3 coatings prepared by RF sputtering on polyethylene separators for high-power lithium ion batteries. Macromol Res 22:1190–1195
36. Song JM, Kang HR, Kim SW, Lee WM, Kim HT (2003) Electrochemical characteristics of phase-separated polymer electrolyte based on poly(vinylidene and ethylene fluoride-*co*-hexafluoropropane) carbonate. Electrochim Acta 48:1339–1346
37. Choi SW, Jo SM, Lee WS, Kim YR (2003) An electrospun poly(vinylidene fluoride) nanofibrous membrane and its battery applications. Adv Mater 15:2027–2032